

1 Inclusive Nucleon Structure Functions

1.1 Overview

Polarized and unpolarized structure functions of the nucleon offer an unique window on the internal quark-structure of stable baryons. Both defining features of QCD, asymptotic freedom at large momenta and small distance scales, as well as confinement and non-perturbative effects at the hadronic scale, can be studied. From measurements of structure functions, we can infer the fraction of the nucleon momentum and spin carried by quarks and (via perturbative evolution) gluons.

After more than three decades of measurements at many labs worldwide, a truly massive amount of data has been collected, covering several decades in both kinematic variables (x , the fraction of the nucleon momentum carried by the struck quark, and the momentum transfer Q^2). However, there are still regions of the kinematic phase space where data are scarce and have large errors, with large improvements possible through experiments at Jefferson Lab with an 11 GeV electron beam.

One of the most interesting open questions is the behavior of the structure functions in the extreme kinematic limit $x \rightarrow 1$, where nearly all of the nucleon momentum is carried by a single quark. We want to understand the relative size of the contribution from both u and d valence quarks as well as quarks with spin parallel and antiparallel to the nucleon spin in this region. Simple phenomenological models like the (SU(6) – symmetric) quark model predict significantly different behavior than perturbative QCD or a quark model with improved hyperfine interaction. One can study this region via the ratio of the neutron over the proton structure function F_2^n/F_2^p and the virtual photon asymmetry A_1 .

Other topics include a detailed study of the phenomenon of “duality”, which is the remarkable agreement between the averaged structure functions in the region of dominant resonant final states with those at much higher final state mass but similar momentum fraction x . This agreement has so far only been shown to exist in the structure function F_2^p , but not for neutrons and not in the longitudinal structure function F_L or the spin structure functions g_1 and g_2 . Finally, both unpolarized and in particular polarized structure functions are still less than well known at low to moderate Q^2 and x . An improved data sample in this region would allow us to study issues like higher twist contributions to the structure functions R and g_2 and maybe also improve perturbative QCD analyses by increasing the Q^2 range covered.

The luminosity-upgraded “CLAS++” will allow us to make significant contributions to these studies, in particular in two cases:

- Measurements of the neutron structure functions F_2^n in the region of very large x , where we can employ a novel technique (recoil proton detection) to disentangle the sought-after signal from nuclear effects, and
- Measurements of polarized structure functions of the proton and deuteron in the region of moderate to high x .

In both cases, the possible luminosity of the experiment is limited by other factors, so that the relatively low luminosity of CLAS is not a disadvantage and can be largely compensated by its very large acceptance.

1.2 Neutron structure functions at large x

1.2.1 Theoretical background

While there exists a large body of data on nucleon structure functions over a wide range of x and Q^2 , the region of large x ($x > 0.6$) is relatively poorly explored. At $x \geq 0.4$ the contributions from the $q\bar{q}$ sea are negligibly small, and the structure functions of the nucleon are dominated by their valence quark content.

Knowledge of the valence quark distributions of the nucleon at large x is vital for several reasons. The simplest SU(6) symmetric quark model predicts that the ratio of d to u quark distributions in the proton is 1/2, however, in nature the breaking of this symmetry results in the d quark distributions being considerably smaller than the u . Various mechanisms have been invoked to explain why the d quark distribution is softer than the u , giving different predictions for the behavior of the d/u ratio as a function of x . For instance, if the interaction between quarks that are spectators to the deep inelastic collision is dominated by one-gluon exchange, then the d quark distribution will be suppressed and the d/u ratio tend to zero in the limit $x \rightarrow 1$ [2]. On the other hand, if the dominant reaction mechanism is that involving DIS from a quark with the same spin orientation as the nucleon, as predicted by perturbative QCD, then the d/u ratio would tend to $\approx 1/5$ as $x \rightarrow 1$ [18]. Determining this ratio experimentally would lead to important insights into the mechanisms responsible for spin-flavor symmetry breaking. In addition, quark distributions at large x are a crucial input for estimating backgrounds in searches for new physics beyond the Standard Model at high energy colliders [4].

Because of the 4:1 weighting of the squared quark charges, data on the proton structure function, F_2^p , provides strong constraints on the u quark distribution at large x ,

$$F_2^p(x) = x \sum_q e_q^2 (q(x) + \bar{q}(x)) \approx x \left(\frac{4}{9} u(x) + \frac{1}{9} d(x) \right). \quad (1)$$

The determination of the d quark distributions, on the other hand, requires in addition the measurement of the neutron structure function, F_2^n . In particular, the ratio d/u can be determined from the ratio F_2^n/F_2^p ,

$$\frac{F_2^n}{F_2^p} \approx \frac{1 + 4d/u}{4 + d/u}, \quad (2)$$

provided $x \geq 0.4$ and sea quark contributions can be neglected.

Because of the absence of free neutron targets, deuterons are usually employed as effective neutron targets. However, at large x theoretical uncertainties in the treatment of nuclear corrections has led to ambiguities in the extracted F_2^n . In particular, inclusion of Fermi motion and nucleon off-shell corrections in the deuteron can lead to values for F_2^n/F_2^p which differ by 50% already at $x = 0.75$ [5, 6]. The differences are even more dramatic if one extracts F_2^n on the basis of the nuclear density model [7].

The measurement of the tagged structure functions in semi-inclusive DIS from the deuteron with a slow recoil proton detected in the backward hemisphere, $e + D \rightarrow e + p + X$, may allow a resolution of this ambiguity [8, 9, 10]. Within the nuclear impulse approximation,

in which the deep inelastic scattering takes place incoherently from individual nucleons, the differential semi-inclusive cross section can be written as

$$\frac{d\sigma}{d^3p} \sim \mathcal{S}(y, p^2) F_2^{n(eff)} \left(\frac{x}{y}, p^2, Q^2 \right), \quad (3)$$

where p is the bound neutron momentum, $\mathcal{S}(y, p^2)$ is the deuteron spectral function, which is obtained from the deuteron wave function, and $F_2^{n(eff)}$ the effective (bound) neutron structure function. The variable y , defined as

$$y = \frac{p \cdot q}{p_d \cdot q/2} \approx \frac{M_d - E_s + p_s^z}{M_d/2} \approx 2 - \alpha_s, \quad (4)$$

where p_s is the spectator proton momentum, gives the light-cone momentum fraction carried by neutron, and is related to the light-cone momentum fraction carried by the spectator proton, $\alpha_s = (E_s - p_s^z)/M$, with $E_s = \sqrt{M^2 + \vec{p}^2}$ and M and M_d the nucleon and deuteron masses, respectively. The effective neutron structure function $F_2^{n(eff)}$ is a function not only of the Bjorken x variable, but also of the nucleon virtuality, p^2 ,

$$p^2 = -\frac{p_T^2}{1-y} - \frac{y}{1-y} (M^2 - M_d^2(1-y)). \quad (5)$$

The p^2 dependence of the $F_2^{n(eff)}$ structure function depends strongly on the theoretical assumptions made about the off-shell behavior of the photon-bound nucleon scattering amplitude. The ratio of the bound to free neutron structure functions in the relativistic, covariant spectator model of Ref.[11] is shown in Fig.1 for several values of x , as a function of the momentum of the spectator, $|\vec{p}|$. While the effect at low $|\vec{p}|$ is small, the deviation from unity increases sharply with increasing momentum, especially at larger values of x where the EMC effect is more pronounced. A similar behavior is observed in the non-relativistic model of Ref.[12], where the assumption of weak binding in the deuteron allows one to calculate the off-shell dependence up to order p^2/M^2 [12].

On the other hand, models such as the color screening model of suppression of point-like configurations (PLC) in bound nucleons [7], which attribute most or all of the EMC effect to a medium modification of the internal structure of the bound nucleon, would predict significantly larger (factor 2 or 3 [10]) deviations from unity than those in Fig. 1. It is important, therefore, that the tagged structure functions be measured in kinematics in which the deviation of $p^2 - M^2$ from zero is as small as possible, to minimize theoretical uncertainties associated with extrapolation to the nucleon pole. Since the deviation of the bound to free structure function ratio from the free limit is roughly proportional to p^2 , sampling the data as a function of p^2 should provide some guidance for a smooth extrapolation to the pole. In practice, considering momentum intervals of 100–200 MeV/c and 200–350 MeV/c would allow the dependence on p^2 to be constrained.

Moreover, recent $(\vec{e}, e'\vec{p})$ polarization transfer experiments at Mainz and Jefferson Lab on ^4He nuclei indicate that the magnitude of the off-shell deformation may be rather small [13]. These experiments measured the ratio of transverse to longitudinal polarization of the ejected protons, which is related to the medium modification of the electric to magnetic

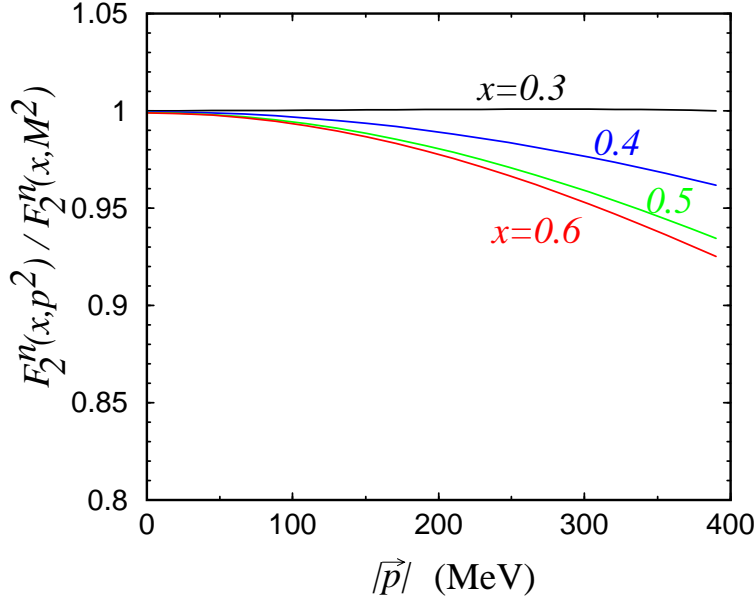


Figure 1: Bound to free neutron structure function ratio as a function of spectator proton momentum (for $p_T=0$), in the model of Ref.[11].

elastic form factor ratio. Using model independent relations derived from quark-hadron duality, one can relate the small, but non-zero medium modification observed in the form factors to a modification at large x of the deep inelastic structure function of the bound nucleon [14], which suggests an effect of $\leq 3\%$ for $x \leq 0.8$.

Another possible source of contamination of the signal is final state interactions (FSI), or rescattering of the spectator proton with the deep-inelastic remnants, X , of the scattered neutron. Extraction of the free neutron structure function in this process is most reliable in the kinematic region where the FSI effects are small, and where different nuclear models for the deuteron spectral function, \mathcal{S} , lead to similar results. The choice of backward angles is designed to minimize these effects. Production of backward protons also suppresses contributions from direct processes, where a nucleon is produced in the γ^*N interaction vertex.

The magnitude of FSI effects has been estimated in Ref.[10] within the framework of the distorted wave impulse approximation (DWIA) [15]. Although a direct calculation of the FSI contribution to the cross section requires knowledge of the full dynamics of the spectator proton- X system, which is currently unavailable, one can estimate the uncertainty introduced through neglect of FSI by comparing with the calculation of FSI effects in the high-energy $d(e, e'p)n$ (break-up) reaction [15]. The effective p - X interaction cross section, σ_{eff} , can be approximated [16] by that extracted from soft neutron production in the high-energy DIS of muons from heavy nuclei [17]. The effects of the FSI is to modify the spectral function $\mathcal{S} \rightarrow \mathcal{S}^{DWIA}$ [15], where

$$\mathcal{S}^{DWIA}(\alpha_s, p_T \approx 0) \sim \mathcal{S}(\alpha_s, p_T \approx 0) \left[1 - \frac{\sigma_{eff}(Q^2, x)}{8\pi \langle r_{pn}^2 \rangle} \frac{|\psi_D(\alpha_s, \langle p_T \rangle)\psi_D(\alpha_s, 0)|}{S(\alpha_s, p_T \approx 0)/\sqrt{E_s E_s(\langle p_T^2 \rangle)}} \right]. \quad (6)$$

Here $\langle r_{pn}^2 \rangle$ is the average separation of the nucleons within the deuteron, E_s is the spectator nucleon energy, and $E_s(\langle p_T^2 \rangle) = \sqrt{M^2 + p_z^2 + \langle p_T^2 \rangle}$ is the energy evaluated at the average transverse momentum $\langle p_T^2 \rangle^{1/2} \sim 200\text{--}300$ MeV/c transferred for the hadronic soft interactions with effective cross section σ_{eff} . The steep momentum dependence of the deuteron wave function, $|\psi_D(\alpha_s, \langle p_T \rangle)| \ll |\psi_D(\alpha_s, p_T \approx 0)|$, ensures that FSI effects are suppressed in the extreme backward kinematics.

The effects of FSI are illustrated in Fig.2, which shows the ratio of the (light-cone) spectral function including FSI effects within the DWIA to that without [10]. At extreme backward kinematics ($p_T \approx 0$) one sees that FSI effects contribute less than $\sim 5\%$ to the overall uncertainty of the $d(e, e'n)X$ cross section for $\alpha_s \geq 1.5$. This number can be considered as an upper limit on the uncertainties due to FSI. At larger p_T (≥ 0.3 GeV/c), and small α_s (≈ 1), the double scattering contribution (which is not present for the extreme backward case 6) plays a more important role in FSI [15].

A further potential problem with Eq.(3) is that at very large x ($x \geq 0.7$) the factorization approximation itself breaks down [11] and higher order corrections to Eq.(3) must be included if one wants accuracy to within a few %. To avoid theoretical ambiguities one should therefore restrict the analysis to spectator momenta below $\approx 150 - 200$ MeV/c.

Of course, in order to identify any residual nuclear effects, it would be ideal to repeat this experiment by detecting spectator neutrons. Comparing the bound proton structure function with the free proton structure function would then allow one to correct the bound neutron structure function for any remaining nuclear effects.

In addition to determining the free neutron structure function, tagged structure function measurements on the deuteron could allow one to discriminate between different hypotheses on the origin of the nuclear EMC effect [10]. In particular, one may be able to distinguish between models in which the effect arises entirely from hadronic degrees of freedom — nucleons and pions, and models in which the effect is attributed to the explicit deformation of the wave function of the bound nucleon itself. By comparing ratios of semi-inclusive cross sections at different values of x , which further reduces the dependence on the deuteron spectral function [7], one can discriminate between models such as the PLC suppression and Q^2 rescaling models, which predict a fast drop with α_s , and nuclear binding models, in which the α_s dependence is quite weak [10]. Finally, these studies would enable one to test the validity of factorization in nuclear DIS, and determine the boundaries of the traditional convolution approach to describing nuclear structure functions.

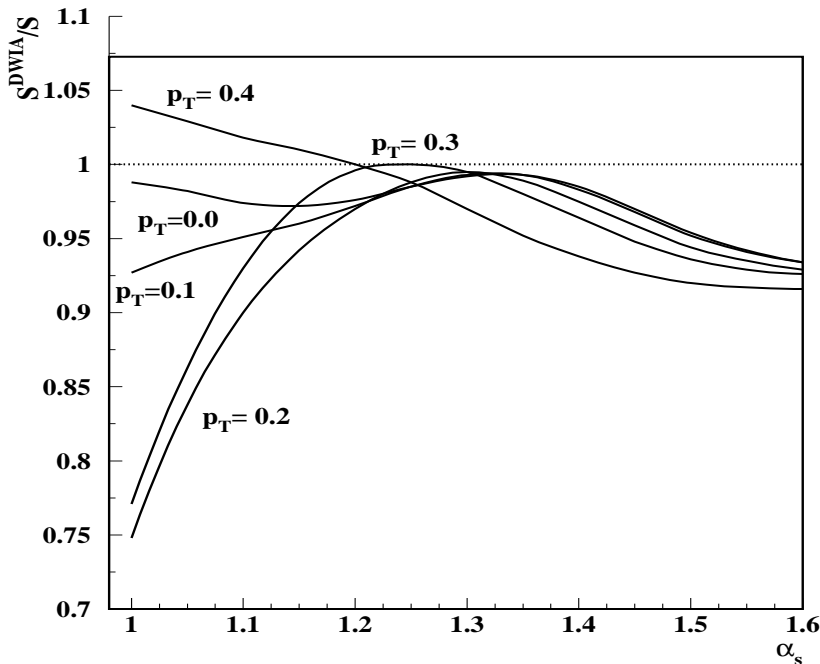


Fig.1

Figure 2: Spectral function calculated with and without FSI effects within the DWIA [10]. The curves correspond to different values of the spectator nucleon transverse momentum (in GeV/c).

1.2.2 Recoil detector

Improvements in rate capability of vertex detectors over the last decades, particularly pushed by the high-energy physics community, enables the new neutron tagging technique we propose. We propose to build a 30 cm long, 20 cm diameter, 5 atm target-detector gas vessel. The inner 10 cm diameter will contain 5 atm deuterium gas that will act as target in the CLAS detector. The surrounding cylindrical detector consists of six layers of Gas Electron Multiplier (GEM)/microstrip detectors, a technology developed by Fabio Sauli at CERN. This detector will operate at a pressure of 5 atm argon gas. A thin aluminized mylar foil is used to separate the 5 atm deuterium gas from the 5 atm argon gas, while an additional gas vessel will be used to permanently maintain zero differential gas pressure. Assuming a beam current of 100 nA, a luminosity of 5×10^{33} electron-atoms/cm²/s is obtained. Please note that in the presented concept one could replace the deuterium target gas by another target gas of choice.

Basically, the GEM is a perforated foil of insulating material coated on both sides with a thin metal layer. The GEM is used as an internal charge preamplification device [34], to overcome the problems encountered when using Micro Strip Gas Chambers (MSGC). With suitable potential applied, the GEM acts as powerful preamplifier for electrons released by ionizing radiation in a gas, transferring most of the multiplied electron charge to a pickup electrode or to another amplifying device. The structure has been the subject of studies aimed at ascertaining its properties in the detection of soft X-rays and charged particles, in the laboratory and in beam conditions [35, 36, 37, 38, 39, 40, 41, 42, 43, 44].

In the proposed detector, each GEM detector has the same standard structure. Primary ionization is produced by radiation in a first drift region, amplified by the GEM. A second, induction, region is used to collect the amplified electrons by the readout boards. Both

drift and induction gas region are a few millimeters thick, and filled with Argon gas. The GEM sheet consists of 50 μm thin insulation foil, with 5 μm copper clad on both sides. The thicknesses and materials we intend to use for this composite detector are all relatively standard, however we are at the limits of the technology in the timing performance of this detector. Decent timing (<10 ns) is required to provide a real to accidental ratio of better than one to one in the tagging process. The outer area of the 5 atm detector will consist of one mm of Al to provide a safety factor of at least four, assuming that we might want to operate at a 10 atm pressure at a later date. Main Research and Development project will be the construction of a high-pressure cylindrical GEM detector.

Realistic simulations indicate the possibility to detect spectator protons with momenta between 70 and 200 MeV/c with this composite detector. The resolution in momentum obtained is less than 7 MeV/c (RMS). The minimum necessary gain for a 5 atm Argon detector is ≤ 20 , whereas gains of over 100 at 7 atm operating pressure have been shown in the laboratory [45]. This minimum necessary gain prescribes how many electrons need to be collected during an integration time to minimize electronic noise related with modern high-density fast electronics.

To suppress possible contamination from protons originating from smaller spectator momenta and transformed to these momenta by the production with slow pions associated with the deep inelastic process, we intend to initially only use the protons in the backward hemisphere, i.e. on the opposite side of the momentum transfer given by the scattered electron [46]. Calculations and analysis of older neutrino data show that this should suppress these reaction mechanism effects sufficiently [47].

This target-detector system will be placed in the proposed CLAS++ solenoid. This solenoid provides a longitudinal field far above the 10 kG longitudinal field we need to protect the inner detectors from low-energy (<1 MeV) Møller electrons.

1.2.3 Expected results

We have simulated the expected results from a 40 day (100% efficient) run at 11 GeV in CLAS++ with the recoil detector as described above. We assumed a minimum momentum of 70 MeV/c for proper detection of a proton going perpendicular to the detector axis, and accordingly more (due to energy loss) for protons at different angles. We used a simple model of the acceptance of both CLAS++ for the scattered electrons and of the recoil detector for protons. To select events where the neutron is close to on-shell, we require that the recoil momentum is less than 180 MeV/c. We also require that the spectator makes an angle of at least 110 degrees with the direction of the momentum transfer vector \mathbf{q} .

Under these conditions, we expect 1.7 M coincident events total, and 700k events with recoil momentum below 100 MeV/c. The average spectator light cone fraction will be $\alpha_S = 1.1$. We will cover a range in W from the elastic peak to about $W = 4$. Restricting the kinematics to $W > 1.8$ GeV (where resonant final states have little influence), we will collect data for x between 0.1 and 0.85, with sufficient statistics to bin in several Q^2 bins from 1 to 13 GeV²/c² and to study the dependence on the recoil momentum.

As an example we show in Fig. 3 the statistical precision we can achieve for the ratio F_2^n/F_2^p at high x . Clearly, the data will allow us (for the first time) to differentiate unambiguously between different expectations for this ratio.

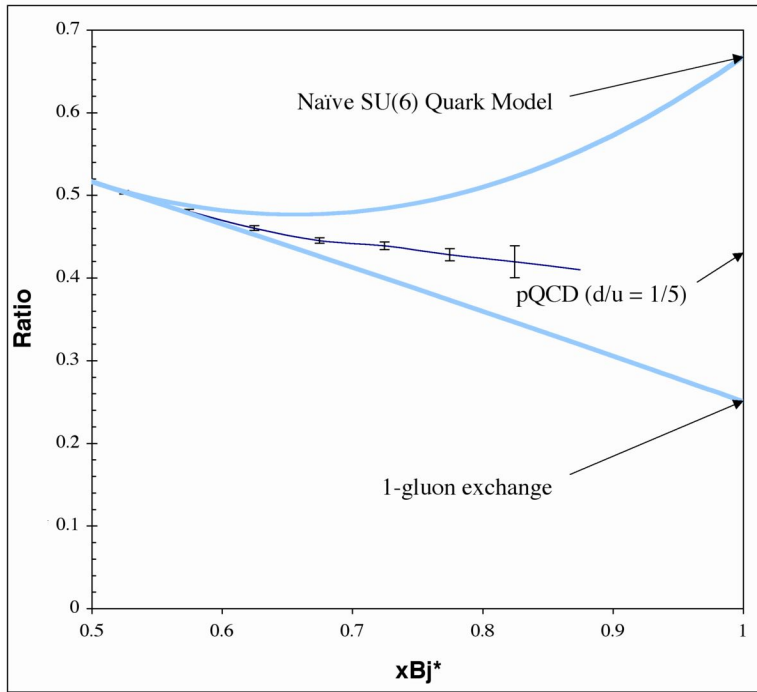


Figure 3: Ratio between the neutron and proton structure functions F_2^n and F_2^p at high x . The lines indicate different possible approaches to the limit $x \rightarrow 1$ which cannot be excluded by present-day data, due to the uncertainty of nuclear effects. The error bars indicate the statistical precision we can achieve in a 40 day run, with full reconstruction of the kinematics via detection of a backwards moving spectator proton .

1.3 Spin structure functions

1.3.1 Measurement goals

While the behavior of the spin-averaged quark distributions at large x still awaits definitive resolution, our lack of understanding of the spin-dependent distributions at large x is even more striking. For instance, there are a number of qualitatively different predictions for the polarization asymmetry $A_{1,N}$, which (in lowest order in the quark-parton model) is given by the ratio of the spin-dependent to spin-averaged quark distributions,

$$A_{1,N}(x) = \frac{\sum_q e_q^2 \Delta q(x)}{\sum_q e_q^2 q(x)}, \quad (7)$$

where e_q is the quark charge. Perturbative QCD predicts that this should approach unity as $x \rightarrow 1$ for proton, neutron and (neglecting nuclear correction) deuteron targets [18]. In contrast, nonperturbative models such as those based on SU(6) spin-flavor symmetry predict that $A_{1,p} = 5/9$, $A_{1,n} = 0$ and $A_{1,d} = 1/3$ [19]. Presently, the world data set is unable to determine the veracity of these predictions.

Although SU(6) symmetry imposes strict relations between the individual quark distributions, such as $\Delta u = -4\Delta d$, in nature this symmetry is strongly broken. Nonperturbative models which break SU(6) symmetry typically involve a hyperfine interaction derived from one-gluon exchange or pion exchange, which has the effect of suppressing the d quark distribution relative to the u [?, 21, 22, 23]. If the u quark dominates the polarization asymmetries as $x \rightarrow 1$, the asymmetries $A_{1,p}$, $A_{1,n}$ and $A_{1,d}$ (in the absence of nuclear effects) will all tend to unity, and distinguishing between the predictions derived from perturbative QCD will require very accurate data at $x \sim 0.6 - 0.8$. On the other hand, the one-gluon exchange model predicts qualitatively different behavior for the individual distributions $\Delta q/q$, especially for the d quark. While the asymptotic $x \rightarrow 1$ limit in perturbative QCD is $\Delta d/d \rightarrow 1$, one-gluon exchange predicts $\Delta d/d \rightarrow -1/3$ as $x \rightarrow 1$, so that even the sign of the prediction differs.

The ratio $\Delta d/d$ can be extracted from semi-inclusive measurements of pions in the current fragmentation region (see section on semi-inclusive processes). A program of inclusive and semi-inclusive double spin asymmetry measurements using an energy upgraded CEBAF in conjunction with polarized proton and deuteron targets can substantially improve our ability to distinguish between the various descriptions of the nucleon.

The large acceptance coverage of CLAS combined with the high luminosity available at an energy upgraded CEBAF will allow access to a large range of x and Q^2 . This will enable precise measurements to be made of moments, or integrals, of the g_1 structure function, and thereby tightly constrain theoretical descriptions of the transition from low to high Q^2 . Understanding this transition is vital for a number of reasons. Through the phenomenon of quark-hadron duality, one can relate the physics of nucleon resonances, which can be described by coherent scattering from constituent quarks at low energy, to the dynamics of single quark scattering which governs the scaling structure function at high energy.

Quark-hadron duality refers to the observation, first made by Bloom and Gilman [24], that the structure function in the resonance region, when suitably averaged over an appropriate energy interval, closely follows the scaling structure function measured at higher energies where the interaction is dominated by non-resonant processes. The duality between descrip-

tions of a nucleon using either quark or hadronic degrees of freedom in different physical processes and under different kinematical conditions is one key to understanding the consequences of QCD for hadronic structure.

While the phenomenon of quark-hadron duality has been observed in the spin-independent F_2 structure function [24, 25], it has not yet been established for spin-dependent structure functions. Because the g_1 structure function is given by a difference of cross sections, which need not be positive, the workings of duality will necessarily be more intricate for g_1 than for the spin-averaged F_2 structure function. Unlike the unpolarized structure functions, spin 1/2 and 3/2 resonances contribute with opposite phase. For fixed Q^2 values less than 1 (GeV/c)² the $\Delta(1232)$ resonance pulls the g_1 structure function below zero, in contrast to the positive value observed in DIS. This is also related to the physics which drives the dramatic variation of the integral of the g_1 structure function from its large and negative value at $Q^2 = 0$ (where it is related to the Gerasimov-Drell-Hearn sum rule) to a positive value at large Q^2 (where it is related to deep inelastic sum rules such as the Bjorken sum rule) [26]. Duality may be realized for polarized structure functions if one averages over a complete set of resonances [27]. To achieve a more complete understanding of duality it is necessary to determine the conditions under which duality occurs in both polarized and unpolarized structure functions.

In the context of QCD, one can relate quark-hadron duality to an operator product expansion of moments of structure functions [28]. According to the twist expansion, moments can be expressed in terms of a power series in $1/Q^2$, where the coefficients of each of the terms in the series are related to matrix elements of quark and gluon operators of a certain twist (which is equal to the difference between the mass dimension and spin of an operator) [29, 30]. The leading, Q^2 -independent term is related to matrix elements of quark bilinear operators, and gives rise to the scaling of the structure function. The higher order terms involve matrix elements of mixed quark-gluon field operators, and characterize the effect on quarks of background color electric and magnetic fields [31]. Because of the $1/Q^2$ suppression, extraction of the higher twist matrix elements, which reflect the role played by quark-gluon correlations in the nucleon, requires structure function moments over a large range of Q^2 , from ~ 0.5 GeV² to several GeV². Measurement of moments of the g_1^p and g_1^d structure functions using CLAS++ would therefore significantly improve our understanding of the workings of QCD at low energy.

Future installation of a transversely polarized target will, in addition, allow measurements of the g_2 structure function, which is the cleanest example of a higher twist effect in the nucleon. Although the g_2 structure function does not have a simple parton model interpretation, the x^2 weighted integral of g_2 is directly related to the color electric and magnetic polarizabilities of the nucleon [31]. Furthermore, the large kinematic coverage of CLAS++ ($0.1 \leq x \leq 0.85$) would allow hitherto unverified sum rules involving g_2 [32, 33] to be accurately tested. A program of transversely polarized structure function measurements would thus open up a whole additional avenue for exploring the transition between asymptotic freedom and confinement physics.

1.3.2 Experimental parameters

For the measurements of spin structure functions in CLAS at 11 GeV, we anticipate that two dedicated polarized targets will be built (see corresponding sections of the technical section of the CDR). Both targets will contain dynamically polarized (DNP) solid ammonia ($^{15}\text{NH}_3$ and $^{15}\text{ND}_3$) at about 1K temperature.

One target will be optimized for longitudinal running. It will be similar to the existing EG1 target, except the Helmholtz coils will be replaced by the new CLAS shielding solenoid. The solenoid will run at its maximum field (5 T), with additional shim coils to create a region of sufficient homogeneity (of order 10^{-4}) over the target cell region. This field will both shield CLAS from Moller electrons and at the same time allow Dynamic Nuclear Polarization of the target samples. The acceptance of this target will fully match the acceptance of the upgraded CLAS.

For the transverse target, we expect to use similar parameters. However, the holding field of 5 Tesla is now sideways (pointing horizontally) which requires a new set of coils, optimized for maximum opening between the coils and closer to the target (to minimize interference with the CLAS coils). We expect a maximum acceptance of ± 20 degrees horizontally and ± 35 degrees vertically. The Moller electrons will be ejected sideways, where they can be contained in massive shielding plates. The electron beam will go through a chicane of one upbending and two downbending magnets, so that it will enter the polarized target pointing down and then being bent into the normal beam line to the electron dump.

For the following rate estimates, we assume 40 ideal running days (corresponding to 3 calendar months) for each target configuration and both NH_3 and ND_3 , and a beam polarization of 70% on average. We expect average target polarizations of 80% for NH_3 and 40% for ND_3 targets, in agreement with recent experience at JLab and SLAC. The overall dilution factor (ratio of events from polarized nucleons to all events) for these targets is about 0.13 for NH_3 and 0.2 for ND_3 , due to the presence of ^{15}N in the ammonia and liquid Helium coolant as well as entrance and exit foils. We will run with about 20 nA beam current, rastered over the surface of the targets of length 1 cm, yielding an overall luminosity of about $5 \cdot 10^{34} \text{ cm}^{-2}\text{s}^{-1}$, similar to the expected unpolarized running conditions. Note that this luminosity is only one order of magnitude lower than the optimum luminosity that can typically be achieved for solid state polarized targets. This makes CLAS a superior choice for measurements with these targets, since the large solid angle (about one steradian) compensates for the limited luminosity and all kinematic points can be measured simultaneously.

1.3.3 Expected results

Text goes here

References

- [1] Upgrading CLAS to Higher Energy

- [2] R.P. Feynman, *Photon Hadron Interactions* (Benjamin, Reading, Massachusetts, 1972); F.E. Close, Phys. Lett. **43** B, 422 (1973); Nucl. Phys. **B80**, 269 (1973); R.D. Carlitz, Phys. Lett. **58** B, 345 (1975); N. Isgur, Phys. Rev. D **59**, 034013 (1999).
- [3] G.R. Farrar and D.R. Jackson, Phys. Rev. Lett. **35**, 1416 (1975).
- [4] S. Kuhlmann *et al.*, Phys. Lett. B **476**, 291 (2000).
- [5] L.W. Whitlow *et al.*, Phys. Lett. B **282**, 475 (1992); A. Bodek, S. Dasu and S. E. Rock, in Tucson Part. Nucl. Phys. 768 (1991).
- [6] W. Melnitchouk and A.W. Thomas, Phys. Lett. B **377**, 11 (1996).
- [7] L. L. Frankfurt and M. I. Strikman, Nucl. Phys. **B250**, 1585 (1985); Phys. Rep. **160**, 235 (1988).
- [8] L. L Frankfurt and M. I. Strikman, Phys. Rep. **76**, 217 (1981).
- [9] S. Simula, Phys. Lett. B **387**, 245 (1996).
- [10] W. Melnitchouk, M. Sargsian and M.I. Strikman, Z. Phys. A **359**, 99 (1997).
- [11] W. Melnitchouk, A.W. Schreiber and A.W. Thomas, Phys. Lett. B **335** (1994) 11; Phys. Rev. D **49**, 1183 (1994).
- [12] S. A. Kulagin, G. Piller and W. Weise, Phys. Rev. C **50**, 1154 (1994); S. A. Kulagin, W. Melnitchouk, G. Piller and W. Weise, Phys. Rev. C **52**, 932 (1995).
- [13] S. Dieterich *et al.*, Phys. Lett. B **500**, 47 (2001); R. Ransome, Nucl. Phys. **A699**, 360 (2002).
- [14] W. Melnitchouk (Jefferson Lab), K. Tsushima, A.W. Thomas, Eur. Phys. J. A **14** (2002), nucl-th/0110071.
- [15] L. L. Frankfurt *et al.*, Z. Phys. A **352**, 97 (1995); Phys. Lett. B **369**, 201 (1996).
- [16] M. I. Strikman, M. Tverskoy, and M. Zhalov, in Proceedings of Workshop “Future Physics at HERA”, Hamburg, pp.1085-1088 (1996), nucl-th/9609055.
- [17] M. R. Adams *et al.*, Phys. Rev. Lett. **74**, 5198 (1995).
- [18] G.R. Farrar and D.R. Jackson, Phys. Rev. Lett. **35**, 1416 (1975).
- [19] F.E. Close, *An Introduction to Quarks and Partons* (Academic Press, 1979).
- [20] F.E. Close, Phys. Lett. **43** B, 422 (1973).
- [21] R.D. Carlitz, Phys. Lett. **58** B, 345 (1975).
- [22] F.E. Close and A.W. Thomas, Phys. Lett. B **212**, 227 (1988).
- [23] N. Isgur, Phys. Rev. D **59**, 034013 (1999).

- [24] E.D. Bloom and F.J. Gilman, Phys. Rev. Lett. **16**, 1140 (1970); Phys. Rev. D **4**, 2901 (1971).
- [25] I. Niculescu *et al.*, Phys. Rev. Lett. **85**, 1182, 1186 (2000).
- [26] V.D. Burkert and B.L. Ioffe, Phys. Lett. B **296**, 223 (1992); J. Exp. Theor. Phys. **78**, 619 (1994).
- [27] F.E. Close and N. Isgur, Phys. Lett. B **509**, 81 (2001).
- [28] A. de Rújula, H. Georgi and H.D. Politzer, Ann. Phys. **103**, 315 (1975).
- [29] X. Ji and P. Unrau, Phys. Rev. D **52**, 72 (1995); X. Ji and W. Melnitchouk, Phys. Rev. D **56**, 1 (1997).
- [30] J. Edelmann, G. Piller, N. Kaiser and W. Weise, Nucl. Phys. **A665**, 125 (2000).
- [31] E. Stein, P. Gornicki, L. Mankiewicz and A. Schafer, Phys. Lett. B **353**, 107 (1995).
- [32] H. Burkhardt and W.N. Cottingham, Ann. Phys. **56**, 453 (1970).
- [33] A.V. Efremov, O.V. Teryaev and E. Leader, Phys. Rev. D **55**, 4307 (1997).
- [34] F. Sauli, Nucl. Instr. and Meth. **A386**, 531 (1997).
- [35] R. Bouclier, M. Capeans, W. Dominik, M. Hoch, J.-C. Labbe, G. Million, L. Ropelewski, F. Sauli, A. Sharma, IEEE Trans. Nucl. Sci. NS-44, 646 (1997).
- [36] R. Bouclier, W. Dominik, M. Houch, J.-C. Labbe, G. Million, L. Ropelewski, F. Sauli, A. Sharma, G. Manzin, Nucl. Instr. and Meth. **A396**, 50 (1997).
- [37] J. Benlloch, A. Bressan, M. Capeans, M. Gruwe, M. Hoch, J.-C. Labbe, A. Placci, L. Ropelewski, F. Sauli, Nucl. Instr. and Meth. **A419**, 410 (1998).
- [38] J. Benlloch, A. Bressan, C. Buttner, M. Capeans, M. Gruwe, M. Hoch, J.-C. Labbe, A. Placci, L. Ropelewski, F. Sauli, A. Sharma, R. Veenhof, IEEE Trans. Nucl. Sci. NS-45, 234 (1998).
- [39] C. Buttner, M. Capeans, W. Dominik, M. Hoch, J.-C. Labbe, G. Manzin, G. Million, L. Ropelewski, F. Sauli, A. Sharma, Nucl. Instr. and Meth. **A409**, 79 (1998).
- [40] W. Beaumont, T. Beckers, J. DeTroy, V. Van Dyck, O. Bouhali, F. Udo, C. VanderVelde, W. Van Doninck, P. Vanlaer, V. Zhukov, Nucl. Instr. and Meth. **A419**, 394 (1998).
- [41] R. Bellazzini, A. Brez, G. Gariano, L. Latronic, N. Lumb, G. Spandre, M.M. Massai, R. Raffo, M.A. Spezziga, Nucl. Instr. and Meth. **A419**, 429 (1998).
- [42] A. Bressan, J.-C. Labbe, P. Pagano, L. Ropelewski, F. Sauli, Nucl. Instr. and Meth. **A425**, 254 (1999).

- [43] A. Bressan, L. Ropelewski, F. Sauli, D. Mormann, T. Muller, H.J. Simonis, Nucl. Instr. and Meth. **A425**, 262 (1999).
- [44] S. Bachmann, A. Bressan, L. Ropelewski, F. Sauli, A. Sharma, D. Mormann, Nucl. Instr. and Meth. **A438**, 376 (1999).
- [45] F. Sauli, private communications.
- [46] S. Simula, private communications.
- [47] G.D. Bosveld, A.E.L. Dieperink, and A.G. Tenner, Phys. Rev. C **49**, 2379 (1994).